

# Performance of Water-based Liquid Scintillator

D. Beznosko<sup>c</sup>, M.V. Diwan<sup>a</sup>, S.Hans<sup>b</sup>, D. Jaffe<sup>a</sup>, S.H. Kettell<sup>a</sup>, R.Rosero<sup>b</sup>,  
H. Themann<sup>a</sup>, B. Viren<sup>a</sup>, E. Worcester<sup>a</sup>, M. Yeh<sup>b</sup>, C. Zhang<sup>a</sup>

<sup>a</sup>*Physics Department, Brookhaven National Laboratory, Upton, NY 11973, USA*

<sup>b</sup>*Chemistry Department, Brookhaven National Laboratory, Upton, NY 11973, USA*

<sup>c</sup>*Department of Physics, Nazarbayev University, Astana, 010000, KZ*

---

## Abstract

The Water-based Liquid Scintillator (WbLS) is a new material currently under development. It is based on the idea of dissolving the organic scintillator in water using special surfactants. This material strives to achieve the novel detection techniques by combining the Cerenkov rings and scintillation light, as well as the total cost reduction compared to pure liquid scintillator (LS).

Presented are the light yield measurements for the three different proton beam energies (210MeV, 475MeV and 2000MeV) for water, two different WbLS formulations (0.4% and 0.99%) and pure LS. The results show that a goal of 100 optical photons/MeV, indicated by the simulation to be an optimal light yield for observing both the Cerenkov ring and scintillation light from the proton decay in a large water detector, has been achieved.

*Keywords:* Water based, liquid scintillator, beam test

---

## 1. Motivation

In large water detectors, the Cerenkov radiation produced by a charged particle above the threshold can be used for particle identification, and the reconstruction of its direction and energy [1]. However, all charged particles below the Cerenkov threshold are missed. Detecting these below-threshold particles is important for various applications. For example, in the search of the proton decay, in the  $p^+ \rightarrow K^+ \bar{\nu}$  channel, where  $K^+$  is mostly below Cerenkov threshold and is invisible in a water detector. The use of the WbLS

---

*Email address:* `dima@dozory.us` (D. Beznosko)

9 makes the kaon visible and allows for the separation of  $K^+$ ,  $\mu^+$  and  $e^+$  signals  
10 using timing and reduce background for this decay channel.

11 In either LS or WbLS, the isotropic scintillation light is produced by  
12 the charged particle energy deposition via ionization, but the scintillator  
13 components may interfere with the Cerenkov ring detection. To detect  $K^+$   
14 and preserve the Cerenkov ring, MC studies indicate that the light yield  
15 (LY) from the scintillator component in the WbLS should be 100 optical  
16 photons/MeV.

17 Thus, WbLS potentially combines both the Cerenkov ring and scintil-  
18 lation light capabilities. It can preserve the particle identification for the  
19 particles above the Cerenkov threshold, and detect the charged particles be-  
20 low the threshold via the scintillation light. In addition, WbLS features the  
21 lower cost than pure LS and it is safer to handle[ask Minfang for reference].

22 The ability to reach the desired LY can be checked using the monoener-  
23 getic proton beam with different WbLS concentrations. For the test, the two  
24 different WbLS formulations (0.4% and 0.99%), pure water and pure LS sam-  
25 ples were chosen. Three different proton beam energies were used with each  
26 sample. The choice of the energies comes from the following considerations:

- 27 • 2000MeV protons behave as minimum ionizing particle (MIP)
- 28 • 475MeV protons are just below the Cerenkov limit in water
- 29 • 210MeV protons have  $\sim$ same energy deposition as  $K^+$  from the proton  
30 decay channel mentioned above.

## 31 2. Experimental Setup

32 The experimental setup used for the proton beam test is shown in (Fig-  
33 ure 1). Two tubs with the samples were used (T1 and T2). Three 2cm x  
34 2cm 5mm thick plastic scintillator hodoscopes were used (H1 to H3) with the  
35 beam trigger being formed by the coincidence of the H1&H2 only. H3 was  
36 intended to verify whether particles exit T2. .

### 37 2.1. Tub and Signal Readout Description

38 Two tubs were used in the experiment:

- 39 • T1 from Polytetrafluoroethylene (PTFE) (white, highly reflective),

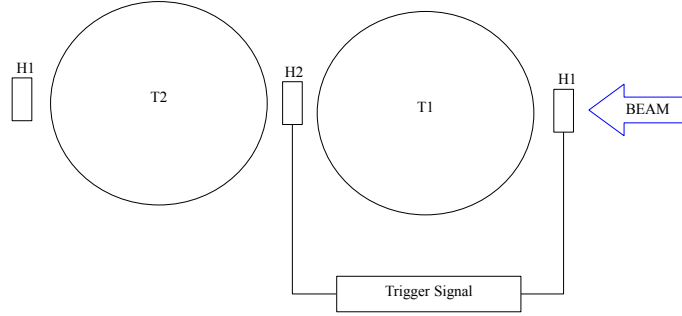


Figure 1: Proton beam test experimental setup.

- T2 from Aluminum, coated with black PTFE (very low reflectivity).

The T1 allows the capture of most of the light produced in the tub, whereas T2 allows for the observation of the light coming directly from the scintillation without the multiple wall reflections. An image of a tub is in (Figure 3). Both T1 and T2 have the same dimensions:

- the lid is 19.05mm thick,
- the walls and bottom are 6.35mm thick,
- inner height and diameter are 150mm.

. A detailed setup readout scheme is shown in (Figure 2). Both tubs were read out by Hamamatsu [2] R7723 2" Photo-multiplier tubes (PMT). A readout was by the 4-channel 14bit CAEN [3] V1729A Flash Analog-to-Digital Converter (FADC). All tubs signals were connected to the FADC via a variable attenuation unit (Phillips Scientific [4] 804) and a variable amplifier unit (Phillips Scientific 778). For the T1 and the T2 readouts, the gain was set to the values of  $\sim 2x$ . The first output from the amplifier goes to the FADC,

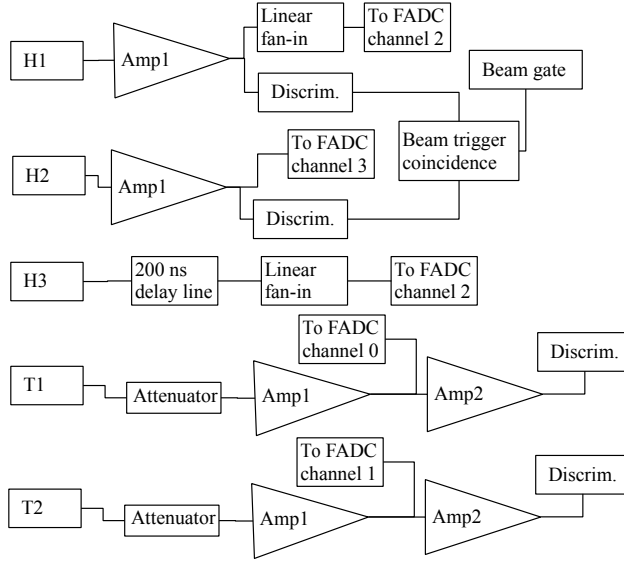


Figure 2: Proton beam test experimental setup.

with a dedicated channel for each tub. The second output from each amplifier channel was used for the single photoelectron (PE) calibration. The gain for the second amplification stage was set at  $\sim 10x$ .

All hodoscopes are also connected via  $\sim 2x$  gain amplifier channels that allows signal splitting. H1 and H3 share the same FADC channel with latter signal being delayed by 200ns. H2 is connected to the last remaining channel of the FADC.

## 2.2. Triggering Scheme

Triggering schema was realized using three 2cm x 2cm, 5mm thick plastic scintillator counters that were readout by 2" PMTs via an air waveguide in order to remove the PMTs from direct beam exposure. The signal from the frontmost and a middle counters were used to form a beam trigger, as indicated in the (Figure 2)

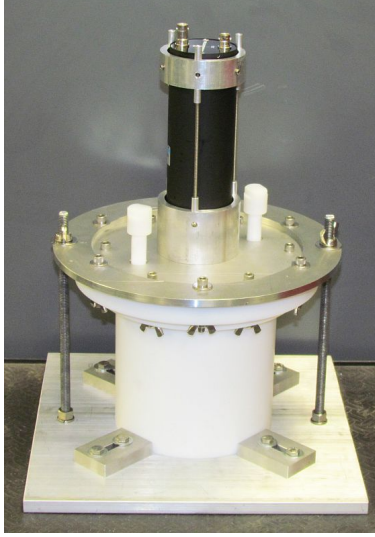


Figure 3: PTFE tub detector with a PMT.

### 69 2.3. Proton Beamline Description

70 A proton test beam was conducted at NASA Space Radiation Laboratory  
 71 (NSRL) facility at BNL. As described above, the three proton beam energies  
 72 were used: 210MeV, 475MeV and 2GeV. The beam had the following main  
 73 characteristics:

- 74 • intensity of  $\sim 1\text{p+}/\text{bunch}$ ,
- 75 • beam size was  $1\text{cm} \times 1\text{cm}$  at 2GeV and  $5.4\text{cm} \times 5.4\text{cm}$  at 210MeV,
- 76 • 0.4s long spills every  $\sim 4$  sec.

## 77 3. Data Analysis

### 78 3.1. Liquids Measured

### 79 3.2. Waveform Analysis

80 The PMT signal is acquired as a waveform shown in (Figure 4). Total  
 81 acquisition window is 2560 bins per event with each bin being 1ns wide; the  
 82 signal is approximately centered and the approximate position is known be-  
 83 forehand. A 300ns window (central one in the figure, between the red and  
 84 blue lines) is used to obtain the integrated signal area by summation. Each

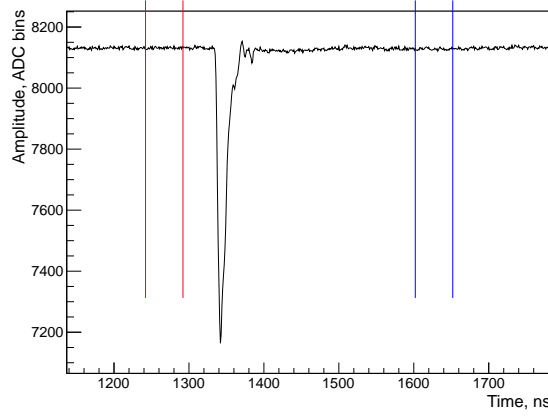


Figure 4: Typical PMT waveform with baseline check windows.

85 point is subtracted from the average baseline to achieve a positive sum. A  
 86 typical signal is smaller than the chosen window width, however, there is a  
 87 small spread in timing of the signals and we want' to be sure that all of the  
 88 signal has been integrated. The size of the chosen window is the same for all  
 89 samples and measurements.

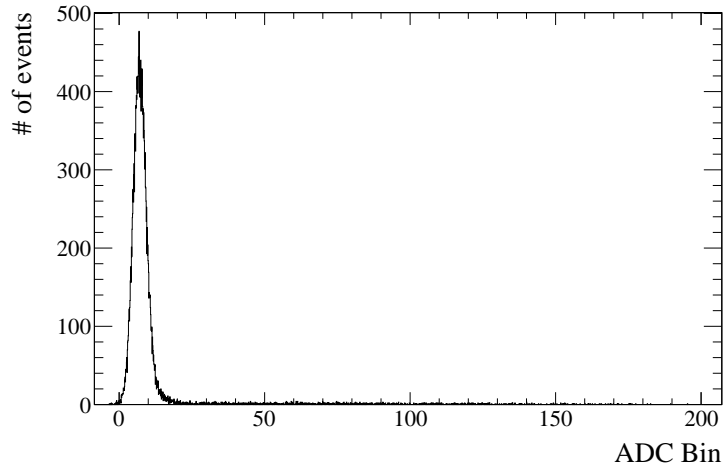


Figure 5: Typical baseline value for a single channel.

90 A baseline is defined as the average value of all the points in the first  
 91 integration window (between the two red lines) that is 50ns wide. A typical

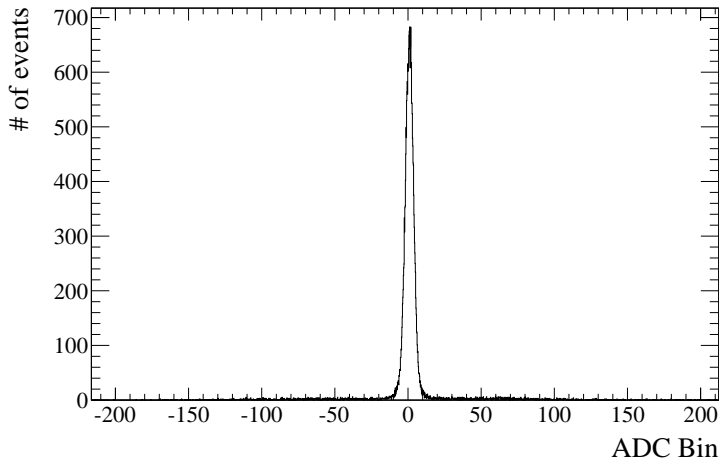


Figure 6: Difference between the baseline and the average of the post-signal window.

baseline is shown in (Figure 5) To check the baseline quality, its averaged value is compared against the average of the post-signal window (between two blue lines). This difference is illustrated in (Figure 6). Events with this difference larger than  $\sim 20$  ADC bins are flagged as bad. This allows for the removal of the noise events or events with the bad baseline. Additionally, a comparison of the baseline with an average of a window at the very beginning of the waveform (between 10ns and 40ns, not shown because the figure is zoomed around the signal area) is used for general baseline quality check using the above criterion.

The integrated area is a measure of total charge that can be converted to the PE yield using the single PE calibration of the PMTs. This allows to describe the measured signals independent of the hardware differences between the channels.

The trigger information that is saved in the two additional FADC channels allows for the offline trigger requirements to be used.

### 3.3. Single Photo Electron Calibration

A single PE calibration was conducted for both signal channels at the end of the test beam run. For it, the trigger is produced from the discriminator that follows the second amplifier for the T1 and T2 signals (separately for each, see Figure 2). The discriminator is set to  $\sim 1/10^{\text{th}}$  of the single PE amplitude as to allow for better PE signal detection efficiency than using

random trigger. Additionally, this forces the PE signal to the signal window region of the FADC output for the simplified analysis and elimination of the partially captured signals. Note that a PE signal is much narrower and lower in amplitude/area than the beam signals that are typically many PEs that arrive with time distribution, thus a smaller integration window is used to reduce noise for cleaner calibration (50ns instead of 300ns).

The signal area calibration is  $168.0 \pm 1.2$  ADC bins and  $132.9 \pm 1.6$  ADC bins for T1 and T2 respectively (the PE signal is summed within the window, so the unit of ADC bin is still used). A special care was taken to separately verify that this method yields the same calibration values as using the light-emitting diode (LED) scheme. For that, calibration runs using the described above scheme and using the dim LED pulses were compared to each other. The LED light level is chosen such that only  $\sim 1/10^{\text{th}}$  of the events has the single PE signal to insure that these are the single photon detection responses.

### 3.4. Light Yield Analysis

#### 3.4.1. Data selection

#### 3.4.2. Energy deposition

Table 1: Energy Deposition in Samples

Beam Energy (MeV)	Sample	T1 Energy Deposit (MeV)	T2 Energy Deposit (MeV)
210	Water, WbLS	70	113
	LS	59	124
475	Water, WbLS	39	42
	LS	34	36
2000	Water, WbLS	28	28
	LS	24	24



131 *3.4.3. Light Yield Results*  
132 *3.5. Systematics*  
133 *3.5.1. Calibration Stability*  
134 **4. Conclusion**

135 **References**

- 136 [1] M. Fechner et.al. (The Super-Kamiokande Collaboration), ‘Kinematic re-  
137 construction of atmospheric neutrino events in a large water Cherenkov  
138 detector with proton identification’, Phys. Rev. D 79 (2009) 112010,  
139 arXiv:0901.1645
- 140 [2] Hamamatsu Photonics, 314-5 Shimokanzo, Toyooka-village, Iwatagun,  
141 Shizuoka-ken, 438-0193 Japan; <http://www.hamamatsu.com>
- 142 [3] CAEN (Costruzioni Apparecchiature Elettroniche Nucleari S.p.A.), Via  
143 della Vetraia 11, 55049 Viareggio, Province of Lucca, Italy, 0584 388398.
- 144 [4] Phillips Scientific, 31 Industrial Ave. Suite 1, Mahwah, N.J. 07430